PERGAMON

Automatica 35 (1999) 3–16

Passive nonlinear observer design for ships using Lyapunov methods: full-scale experiments with a supply vessel[1]

Thor I. Fossen*, Jann Peter Strand

Department of Engineering Cybernetics, Norwegian University of Science and Technology, N-7034 Trondheim, Norway

Received 4 April 1997; revised 25 November 1997; received in final form 12 May 1998

Abstract

Dynamic positioning (DP) and tracking systems for ships are usually designed under the assumption that the kinematic equations can be linearized about a set of predefined constant yaw angles, typically 36 operating points in steps of 10°, to cover the whole heading envelope. This is necessary when applying linear (Kalman filter) theory and gain scheduling techniques. However, global exponential stability (GES) cannot be guaranteed if linear theory is used. In this paper a nonlinear observer is derived. The observer is proven to be passive and GES. The number of tuning parameters is reduced to a minimum by using passivity theory. This results in a simple and intuitive tuning procedure. The proposed observer includes features like estimation of both the low-frequency position and velocity of the ship from noisy position measurements, bias state estimation (environmental disturbances) and wave filtering. The nonlinear passive observer has been simulated on a computer model of a supply vessel and implemented on full-scale ships with excellent results.

Keywords: Nonlinear observers; Passive elements; Marine systems; Ship control

1. Introduction

Dynamic positioning (DP) systems have been commercially available for marine vessels since the 1960s. The first DP systems were designed using conventional PID controllers in cascade with low-pass and/or notch filters to suppress the wave-induced motion components. From the middle of the 1970s, more advanced control techniques based on optimal control and Kalman-filter theory were proposed by Balchen et al. (1976). This work has later been modified and extended by Balchen et al. (1980a, b), Grimble et al. (1980a, b), Fung and Grimble (1983), Sælid et al. (1983) and more lately by Fossen et al. (1996) and Sørensen et al. (1996).

Filtering and state estimation are important features of a DP system. In most cases, measurements of the vessel velocities are not available. Hence, estimates of the velocities must be computed from noisy position and heading measurements through a state observer. Unfortunately, the position and heading measurements are corrupted with colored noise due to wind, waves and ocean currents as well as sensor noise. However, only the slowly varying disturbances should be counteracted by the propulsion system, whereas the oscillatoric motion due to the waves (first-order wave disturbances) should not enter the feedback loop. This is done by using so-called wave filtering techniques, which separate the position and heading measurements into a low-frequency (LF) and wave frequency (WF) position and heading estimate (Fossen, 1994).

In existing DP systems the wave filtering and state estimation problems are solved by using linear Kalman filters. The major drawback of this approach is that the kinematic equations of motions must be linearized about a set of predefined constant yaw angles, typically 36 operating points in steps of 10°, to cover the whole heading envelope. For each of these linearized models, optimal Kalman filter and feedback control gains are computed such that the gains can be modified on-line by using gain-scheduling techniques. In the seek for new control strategies the linear Kalman filter approach is

*Corresponding author. Tel.: + 47 73 59 4361; fax: + 47 73 59 4399; e-mail: tif@itk.ntnu.no. This work was partially supported by ABB Industri, Marine Division and the Norwegian Research Council.

[1]This paper was not presented at any IFAC meeting. This paper was recommended for publication in revised form by Associate Editor J. Z. Sasiadek under the direction of Editor K. Furuta.

0005-1098/99/$—see front matter
PII: S0005-1098(98)00121-6

a major obstacle since it is difficult and time-consuming to tune the state estimator (stochastic system with 15 states and 120 covariance equations). The main reason for this, is that the numerous covariance tuning parameters may be difficult to relate to physical quantities resulting in a somewhat *ad hoc* tuning procedure.

In this paper a nonlinear passive observer is proposed. The observer includes wave filtering properties, bias state estimation, reconstruction of the LF motion components and noise-free estimates of the nonmeasured vessel velocities. The proposed observer is proven to be passive and globally exponentially stable (GES). Hence, only one set of observer gains are needed to cover the whole state space. In addition, the number of observer tuning parameters are significantly reduced and the wave filter parameters are directly coupled to the dominating wave frequency. Passivity theory showed to be a new tool with respect to accurate tuning of the observer. The proposed nonlinear observer opens for new controller designs more in line with the actual structure of the physical system, e.g. by using the *separation principle* (Loria et al., 1998) or *observer backstepping*.

In Fossen and Grøvlen (1998), the concept of vectorial observer backstepping has been applied to derive a GES output feedback control system for ships. This work is, however, based on a simplified model of the environmental disturbances since it is assumed that the WF motion and bias states can be neglected in the design. More recently, Aarset et al. (1998) have shown that these results can be extended to the general case by including a dynamic model for wave filtering and bias state estimation. The main difference between the observer backstepping design and the nonlinear observer presented in this paper is that passivity is not guaranteed in the observer backstepping case. We believe that this is an important feature since passivity arguments will simplify the tuning procedure significantly. Hence, the time needed for sea trials and tuning will be reduced.

The performance and robustness of the observer are demonstrated by computer simulations and full-scale experiments of a thruster controlled supply vessel in the North Sea. The simulation study verifies that all estimation errors converge exponentially to zero. The nonlinear passive observer, as opposed to a linearized Kalman filter, guarantees exponential convergence of all bias estimation errors to zero. This is almost impossible to obtain in commercial DP systems using linearized Kalman filters.

2. Mathematical modelling of ships

2.1. Kinematic equations of motion

Let the earth-fixed position (x, y) and heading ψ of the vessel relative to an earth-fixed frame $X_E Y_E Z_E$ be expressed in vector form by $\boldsymbol{\eta} = [x, y, \psi]^T$, and let the velocities decomposed in a vessel-fixed reference frame be represented by the state vector $\boldsymbol{v} = [u, v, r]^T$. These three modes are referred to as the *surge*, *sway* and *yaw* modes of a ship. The origin of the vessel-fixed frame XYZ is located at the vessel centreline in a distance x_G from the center of gravity (see Fig. 1). The transformation between the vessel-fixed and the earth-fixed velocity vectors is

$$\dot{\boldsymbol{\eta}} = \boldsymbol{J}(\boldsymbol{\eta})\boldsymbol{v} \tag{1}$$

where $\boldsymbol{J}(\boldsymbol{\eta})$ is a state-dependent transformation matrix. Conventional ships are not equipped with actuators in roll and pitch which suggests that the roll and pitch modes should be omitted when designing output feedback controllers for ships. In fact, this is an appropriate assumption since both the rolling and pitching motions of a ship is oscillatoric with zero mean and limited amplitude. Moreover, a conventional ship is *metacentric stable* which implies that there exist restoring moments in roll and pitch. In the remaining of the paper, it is assumed that the ship is sufficient *metacentric stable* such that only the rotation matrix in yaw can be used to describe the kinematic equations of motion, that is

$$\boldsymbol{J}(\boldsymbol{\eta}) = \boldsymbol{J}(\psi) = \begin{bmatrix} \cos\psi & -\sin\psi & 0 \\ \sin\psi & \cos\psi & 0 \\ 0 & 0 & 1 \end{bmatrix}, \tag{2}$$

where $\boldsymbol{J}(\psi)$ is nonsingular for all ψ. Notice that $\boldsymbol{J}^{-1}(\psi) = \boldsymbol{J}^T(\psi)$.

2.2. Ship modelling

The LF motion of a large class of surface ships can be described by the following model (Fossen, 1994):

$$\boldsymbol{M}\dot{\boldsymbol{v}} + \boldsymbol{D}\boldsymbol{v} = \boldsymbol{\tau} + \boldsymbol{J}^T(\boldsymbol{\eta})\boldsymbol{b}, \tag{3}$$

$$\boldsymbol{\tau} = \boldsymbol{B}_u\boldsymbol{u}. \tag{4}$$

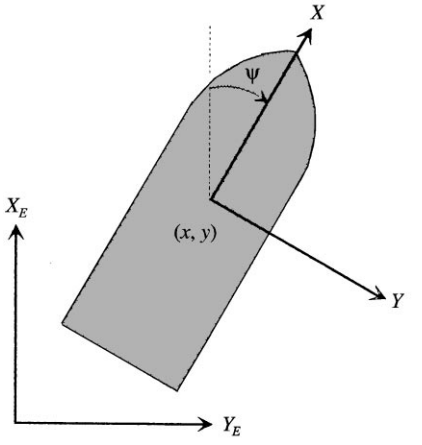

Fig. 1. Definition of the earth-fixed $X_E Y_E Z_E$ and the vessel-fixed XYZ reference frames.

Here $\tau \in \Re^3$ is a control vector of forces and moment provided by the propulsion system, that is main propellers aft of the ship and thrusters which can produce surge and sway forces as well as a yaw moment. In addition to this, ships can be equipped with control surfaces and rudders. The control inputs are denoted by $\boldsymbol{u} \in \Re^r$ ($r \geq 3$) and $\boldsymbol{B}_u \in \Re^{3\times r}$ is a constant matrix describing the actuator configuration. Unmodeled external forces and moment due to wind, currents and waves are lumped together into an earth-fixed constant (or slowly varying) bias term $\boldsymbol{b} \in \Re^3$.

If a small *Froude number* is assumed, the inertia matrix $\boldsymbol{M} \in \Re^{3\times 3}$ which includes hydrodynamic added inertia can be written (Fossen, 1994):

$$\boldsymbol{M} = \begin{bmatrix} m - X_{\dot{u}} & 0 & 0 \\ 0 & m - Y_{\dot{v}} & mx_G - Y_{\dot{r}} \\ 0 & mx_G - N_{\dot{v}} & I_z - N_{\dot{r}} \end{bmatrix}, \tag{5}$$

where m is the vessel mass and I_z is the moment of inertia about the vessel-fixed z-axis. For control applications which are restricted to low-frequency motions, wave frequency independence of added inertia (zero wave frequency) can be assumed. This implies that $\dot{\boldsymbol{M}} = \boldsymbol{0}$. The zero-frequency added mass in surge, sway and yaw due to accelerations along the corresponding axes are defined as $X_{\dot{u}} < 0$, $Y_{\dot{v}} < 0$ and $N_{\dot{r}} < 0$, whereas the cross-terms $Y_{\dot{r}}$ and $N_{\dot{v}}$ can have both signs (SNAME, 1950).

For a *straight-line stable* ship, $\boldsymbol{D} \in \Re^{3\times 3}$ will be a strictly positive damping matrix due to linear wave drift damping and laminar skin friction. The linear damping matrix is defined as (Fossen, 1994)

$$\boldsymbol{D} = \begin{bmatrix} -X_u & 0 & 0 \\ 0 & -Y_v & mu_0 - Y_r \\ 0 & -N_v & mx_G u_0 - N_r \end{bmatrix}, \tag{6}$$

where the cruise-speed $u_0 = 0$ in DP and $u_0 > 0$ when moving forward. In general the damping forces will be nonlinear. However, for DP and cruising at constant speed linear damping is a good assumption since this a regulation problem (Fossen, 1994).

2.3. Bias modelling (slowly varying environmental disturbances)

It is assumed that the bias forces in surge and sway, and the yaw moment are slowly varying. A frequently used bias model for marine control applications is the first-order Markow process

$$\dot{\boldsymbol{b}} = -\boldsymbol{T}^{-1}\boldsymbol{b} + \boldsymbol{\Psi}\boldsymbol{n}, \tag{7}$$

where $\boldsymbol{b} \in \Re^3$ is a vector of bias forces and moment, $\boldsymbol{n} \in \Re^3$ is a vector of zero-mean Gaussian white noise, $\boldsymbol{T} \in \Re^{3\times 3}$ is a diagonal matrix of positive bias time constants and $\boldsymbol{\Psi} \in \Re^{3\times 3}$ is a diagonal matrix scaling the amplitude of $\boldsymbol{n}$. This model can be used to describe slowly-varying environmental forces and moments due to (Fossen, 1994)

- second-order wave drift,
- ocean currents,
- wind,
- unmodeled dynamics.

2.4. First-order wave-induced model

A linear wave frequency (WF) model of order p can in general be expressed as

$$\dot{\boldsymbol{\xi}} = \boldsymbol{\Omega}\boldsymbol{\xi} + \boldsymbol{\Sigma}\boldsymbol{w}, \tag{8}$$

$$\boldsymbol{\eta}_w = \boldsymbol{\Gamma}\boldsymbol{\xi}, \tag{9}$$

where $\boldsymbol{\xi} \in \Re^{3p}$, $\boldsymbol{w} \in \Re^3$ and $\boldsymbol{\Omega}$, $\boldsymbol{\Sigma}$ and $\boldsymbol{\Gamma}$ are constant matrices of appropriate dimensions. The WF response of the ship is generated by using the principle of linear superposition, that is the first-order wave-induced motion $\boldsymbol{\eta}_w = [x_w, y_w, \psi_w]^{\mathrm{T}}$ is added to the LF motion components of the ship given by $\boldsymbol{\eta} = [x, y, \psi]^{\mathrm{T}}$. Hence, the total ship motion is the sum of the LF-motion components and the WF-motion components as shown in Fig. 2. Notice the oscillatoric behavior of the wave-induced motion component. It is assumed that the WF model excitations $\boldsymbol{w}$ in Eq. (8) are zero-mean Gaussian white noise.

For notational simplicity, a second-order wave model for the first-order wave-induced motion is considered in the remaining of the paper. However, higher order wave transfer function approximations can also be used, such as a fourth-order wave model with five parameters, see Grimble et al. (1980a) and Fung and Grimble (1983), and a sixth-order wave model with four parameters (Triantafyllou et al. 1983). The main reason for choosing a higher order of the WF model is that a more precise

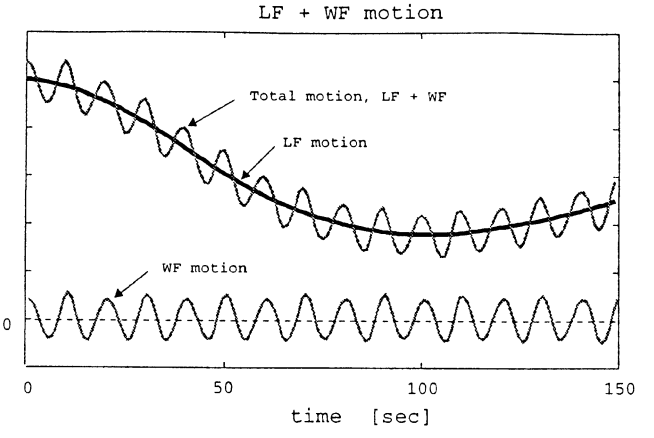

Fig. 2. The total ship motion as the sum of the LF-motion and the WF-motion. Notice that the first-order WF-motion is osillatoric.

approximation to the actual wave spectrum, e.g. the Pierson–Moskowitz or the JONSWAP spectra can be obtained (Fossen, 1994). However, this also increases the number of model parameters to be determined and the dimension of the observer gain matrices to be tuned.

2.4.1. Wave spectrum approximation (second-order wave-induced motion)

The second-order wave-induced motion model was originally proposed by Balchen et al. (1976) who used three harmonic oscillators. Sælid et al. (1983) improved the WF model approximation by including an additional damping term. This model can be written (one model for each degrees of freedom):

$$h_w^i(s) = \frac{\sigma_i s}{s^2 + 2\zeta_i \omega_{0i} s + \omega_{0i}^2}, \tag{10}$$

where ω_{0i} $(i = 1–3)$ is the dominating wave frequency, $\zeta_i (i = 1–3)$ is the relative damping ratio and $\sigma_i (i = 1–3)$ a parameter related to the wave intensity.

A state-space realization of Eq. (10) in three degrees of freedom (DOF) is

$$\begin{bmatrix} \dot{\boldsymbol{\xi}}_1 \\ \dot{\boldsymbol{\xi}}_2 \end{bmatrix} = \begin{bmatrix} \mathbf{0} & \mathbf{I} \\ \boldsymbol{\Omega}_{21} & \boldsymbol{\Omega}_{22} \end{bmatrix} \begin{bmatrix} \boldsymbol{\xi}_1 \\ \boldsymbol{\xi}_2 \end{bmatrix} + \begin{bmatrix} \mathbf{0} \\ \boldsymbol{\Sigma}_2 \end{bmatrix} \boldsymbol{w}, \tag{11}$$

$$\boldsymbol{\eta}_w = [\mathbf{0} \quad \boldsymbol{I}] \begin{bmatrix} \boldsymbol{\xi}_1 \\ \boldsymbol{\xi}_2 \end{bmatrix},$$

where $\boldsymbol{\xi}_1 \in \Re^3$, $\boldsymbol{\xi}_2 \in \Re^3$ and

$$\boldsymbol{\Omega}_{21} = -\operatorname{diag}\{\omega_{01}^2, \omega_{02}^2, \omega_{03}^2\},$$

$$\boldsymbol{\Omega}_{22} = -\operatorname{diag}\{2\zeta_1\omega_{01}, 2\zeta_2\omega_{02}, 2\zeta_3\omega_{03}\},$$

$$\boldsymbol{\Sigma}_2 = \operatorname{diag}\{\sigma_1, \sigma_2, \sigma_3\}.$$

2.5. Measurement system

For conventional ships, only position and heading measurements are available. Several position measurement systems are commercially available, such as hydroaccustic positioning reference (HPR) systems and satellite navigation systems. The two commercial available satellite systems are Navstar GPS (USA) and GLONASS (Russian); see Parkinson (1996). The accuracy of the GPS satellite navigation system is degraded for civilian users and this results in root-mean-square errors of about 50 m for the horizontal positions. However, for ship positioning systems this problem is usually circumvented by using a *differential* global positioning system (DGPS). The main idea of a *differential* GPS system is that a fixed receiver, e.g. located *on shore* with known position, is used to calculate the GPS position errors. The position errors are then transmitted to the GPS-receiver on board of the ship and used as corrections to the actual ship position. In a DGPS-system, the horizontal positioning errors are squeezed down to less than 1 m which is the typical accuracy of a ship positioning system today (Hofmann-Wellenhof et al., 1994).

The heading of the vessel is usually measured by using a gyro compass where gyro drift can be compensated for by using a magnetic compass. The accuracy of a gyro compass is typically in the magnitude of 0.1°.

Hence, the position and heading measurement equation can be written:

$$\boldsymbol{y} = \boldsymbol{\eta} + \boldsymbol{\eta}_w + \boldsymbol{d}, \tag{12}$$

where $\boldsymbol{\eta}_w$ is the vessel's WF motion due to first-order wave-induced disturbances and $\boldsymbol{d} \in \Re^3$ is zero-mean Gaussian white measurement noise. It is important that the observer is tuned such that the observer gains reflect the differences in the noise levels of the measured signals.

In addition to these measurements, the ship observer needs actuator measurements $\boldsymbol{u}$ such that the control forces in surge and sway, and moment in yaw:

$$\boldsymbol{\tau} = \boldsymbol{B}_u \boldsymbol{u} \tag{13}$$

can be computed. Recall that the input matrix $\boldsymbol{B}_u$ is assumed to be known.

Definition 1 (*Wave filtering*). Wave filtering can be defined as the reconstruction of the LF motion components $\boldsymbol{\eta}$ from the noisy measurement $\boldsymbol{y} = \boldsymbol{\eta} + \boldsymbol{\eta}_w + \boldsymbol{d}$ by means of an observer (state estimator). In addition to this, a noise-free estimate of the LF velocity $\boldsymbol{v}$ should be produced from $\boldsymbol{y}$. This is crucial in ship motion control systems since the oscillatoric motion $\boldsymbol{\eta}_w$ due to first-order wave-induced disturbances will, if it enters the feedback loop, cause wear and tear of the actuators and increase the fuel consumption.

Remark 1. In general, it is impossible to counteract the first-order wave-induced motion of a ship when applying a reasonable propulsion and thruster system. Hence, no improvement in position performance should be expected by feeding back the signal $\boldsymbol{\eta}_w$ to the controller.

3. Resulting system model

In the Lyapunov stability analysis, the following assumptions are made:

A1: $\boldsymbol{M} = \boldsymbol{M}^{\mathrm{T}} > \mathbf{0}$. This is true if starboard and port symmetries, and low speed are assumed. Symmetry and positive definiteness are only necessary in the Lyapunov analysis. In addition to this, it is assumed that the added mass terms are independent of the wave-frequency such that $\dot{\boldsymbol{M}} = \mathbf{0}$ holds. This is a good assumption for most low-speed applications (Fossen, 1994).

A2: $\boldsymbol{n} = \boldsymbol{w} = \boldsymbol{0}$. The bias and wave models are driven by zero-mean Gaussian white noise. These terms are omitted in the observer model and Lyapunov function analysis since the estimator states are driven by the estimation error instead.

A3: $\boldsymbol{d} = \boldsymbol{0}$. Zero mean Gaussian white measurement noise is not included in the Lyapunov function since this term is negligible compared to the first-order wave disturbances $\boldsymbol{\eta}_w$. Full-scale experiments have shown that the observer is highly robust for measurement noise produced by commercially available DGPS-systems and gyro compasses.

A4: $\boldsymbol{J}(\boldsymbol{\eta}) = \boldsymbol{J}(\boldsymbol{y})$ or $\boldsymbol{J}(\psi) = \boldsymbol{J}(\psi + \psi_w)$. This is a good assumption since the magnitude of the wave-induced yaw disturbance ψ_w will be less than 5° in extreme weather situations (sea state codes 5–10), and less than 1° during normal operation of the ship (sea state codes 1–5).

Application of Assumptions A1–A4 to Eqs. (1), (3), (7), (11) and (12) yields the following system model:

$$\dot{\boldsymbol{\xi}} = \boldsymbol{\Omega}\boldsymbol{\xi}, \tag{14}$$

$$\dot{\boldsymbol{\eta}} = \boldsymbol{J}(\boldsymbol{y})\boldsymbol{v}, \tag{15}$$

$$\dot{\boldsymbol{b}} = -\boldsymbol{T}^{-1}\boldsymbol{b}, \tag{16}$$

$$\boldsymbol{M}\dot{\boldsymbol{v}} = -\boldsymbol{D}\boldsymbol{v} + \boldsymbol{J}^{\mathrm{T}}(\boldsymbol{y})\boldsymbol{b} + \boldsymbol{\tau}, \tag{17}$$

$$\boldsymbol{y} = \boldsymbol{\eta} + \boldsymbol{\eta}_w = \boldsymbol{\eta} + \boldsymbol{\Gamma}\boldsymbol{\xi}. \tag{18}$$

For notational simplicity, Eqs. (14), (15) and (18) are written in state-space form:

$$\dot{\boldsymbol{\eta}}_0 = \boldsymbol{A}_0\boldsymbol{\eta}_0 + \boldsymbol{B}_0\boldsymbol{J}(\boldsymbol{y})\boldsymbol{v}, \tag{19}$$

$$\boldsymbol{y} = \boldsymbol{C}_0\boldsymbol{\eta}_0, \tag{20}$$

where $\boldsymbol{\eta}_0 = [\boldsymbol{\xi}^{\mathrm{T}}, \boldsymbol{\eta}^{\mathrm{T}}]^{\mathrm{T}}$ and

$$\boldsymbol{A}_0 = \begin{bmatrix} \boldsymbol{\Omega} & \boldsymbol{0} \\ \boldsymbol{0} & \boldsymbol{0} \end{bmatrix}, \qquad \boldsymbol{B}_0 = \begin{bmatrix} \boldsymbol{0} \\ \boldsymbol{I} \end{bmatrix}, \qquad \boldsymbol{C}_0 = [\boldsymbol{\Gamma} \quad \boldsymbol{I}]. \tag{21}$$

4. Nonlinear observer design

The objective of the observer design is to generate LF position and heading estimates, estimates of the unmeasured LF velocities and estimates of the bias terms by using the idea of wave filtering as stated in Definition 1. Since the measurements consist of both a LF and a WF component, a wave model is included in the observer to produce a notch effect. When the dominating wave frequency is known, the observer should have the properties of a notch filter in the frequency range of the wave disturbances. Notice that the notch frequency (dominating wave frequency) will be inside the bandwidth of most ships.

4.1. Observer equations

A nonlinear observer copying the dynamics (14)–(18) is

$$\dot{\hat{\boldsymbol{\xi}}} = \boldsymbol{\Omega}\hat{\boldsymbol{\xi}} + \boldsymbol{K}_1\tilde{\boldsymbol{y}}, \tag{22}$$

$$\dot{\hat{\boldsymbol{\eta}}} = \boldsymbol{J}(\boldsymbol{y})\hat{\boldsymbol{v}} + \boldsymbol{K}_2\tilde{\boldsymbol{y}}, \tag{23}$$

$$\dot{\hat{\boldsymbol{b}}} = -\boldsymbol{T}^{-1}\hat{\boldsymbol{b}} + \frac{1}{\gamma}\boldsymbol{\Lambda}\tilde{\boldsymbol{y}}, \tag{24}$$

$$\boldsymbol{M}\dot{\hat{\boldsymbol{v}}} = -\boldsymbol{D}\hat{\boldsymbol{v}} + \boldsymbol{J}^{\mathrm{T}}(\boldsymbol{y})\hat{\boldsymbol{b}} + \boldsymbol{\tau} + \frac{1}{\gamma}\boldsymbol{J}^{\mathrm{T}}(\boldsymbol{y})\mathcal{K}\tilde{\boldsymbol{y}}, \tag{25}$$

$$\hat{\boldsymbol{y}} = \hat{\boldsymbol{\eta}} + \boldsymbol{\Gamma}\hat{\boldsymbol{\xi}}, \tag{26}$$

where $\tilde{\boldsymbol{y}} = \boldsymbol{y} - \hat{\boldsymbol{y}}$ is the estimation error and $\boldsymbol{K}_1 \in \Re^{6\times 3}$, $\boldsymbol{K}_2 \in \Re^{3\times 3}$, $\mathcal{K} \in \Re^{3\times 3}$ and $\boldsymbol{\Lambda} \in \Re^{3\times 3}$ are observer gain matrices to be interpreted later. $\gamma > 0$ is an additional scalar tuning parameter motivated by the Lyapunov analysis, see Section 5.1. Similarly as Eqs. (19) and (20), the system (22), (23) and (26) is written in state-space form:

$$\dot{\hat{\boldsymbol{\eta}}}_0 = \boldsymbol{A}_0\hat{\boldsymbol{\eta}}_0 + \boldsymbol{B}_0\boldsymbol{J}(\boldsymbol{y})\hat{\boldsymbol{v}} + \boldsymbol{K}\tilde{\boldsymbol{y}}, \tag{27}$$

$$\hat{\boldsymbol{y}} = \boldsymbol{C}_0\hat{\boldsymbol{\eta}}_0, \tag{28}$$

where $\hat{\boldsymbol{\eta}}_0 = [\hat{\boldsymbol{\xi}}^{\mathrm{T}}, \hat{\boldsymbol{\eta}}^{\mathrm{T}}]^{\mathrm{T}}$ and

$$\boldsymbol{K} = \begin{bmatrix} \boldsymbol{K}_1 \\ \boldsymbol{K}_2 \end{bmatrix}. \tag{29}$$

The observer structure is shown in Fig. 3.

4.2. Estimation error dynamics

The estimation errors are defined as $\tilde{\boldsymbol{v}} = \boldsymbol{v} - \hat{\boldsymbol{v}}$, $\tilde{\boldsymbol{b}} = \boldsymbol{b} - \hat{\boldsymbol{b}}$ and $\tilde{\boldsymbol{\eta}}_0 = \boldsymbol{\eta}_0 - \hat{\boldsymbol{\eta}}_0$. Hence, the error dynamics can be written:

$$\dot{\tilde{\boldsymbol{\eta}}}_0 = (\boldsymbol{A}_0 - \boldsymbol{K}\boldsymbol{C}_0)\tilde{\boldsymbol{\eta}}_0 + \boldsymbol{B}_0\boldsymbol{J}(\boldsymbol{y})\tilde{\boldsymbol{v}}, \tag{30}$$

$$\dot{\tilde{\boldsymbol{b}}} = -\boldsymbol{T}^{-1}\tilde{\boldsymbol{b}} - \frac{1}{\gamma}\boldsymbol{\Lambda}\tilde{\boldsymbol{y}}, \tag{31}$$

$$\boldsymbol{M}\dot{\tilde{\boldsymbol{v}}} = -\boldsymbol{D}\tilde{\boldsymbol{v}} + \boldsymbol{J}^{\mathrm{T}}(\boldsymbol{y})\tilde{\boldsymbol{b}} - \frac{1}{\gamma}\boldsymbol{J}^{\mathrm{T}}(\boldsymbol{y})\mathcal{K}\tilde{\boldsymbol{y}}. \tag{32}$$

The dynamics of the velocity estimation error (32) can be rewritten as

$$\boldsymbol{M}\dot{\tilde{\boldsymbol{v}}} = -\boldsymbol{D}\tilde{\boldsymbol{v}} - \frac{1}{\gamma}\boldsymbol{J}^{\mathrm{T}}(\boldsymbol{y})\tilde{\boldsymbol{z}},$$

where

$$\tilde{\boldsymbol{z}} \triangleq \mathcal{K}\tilde{\boldsymbol{y}} - \gamma\tilde{\boldsymbol{b}}. \tag{33}$$

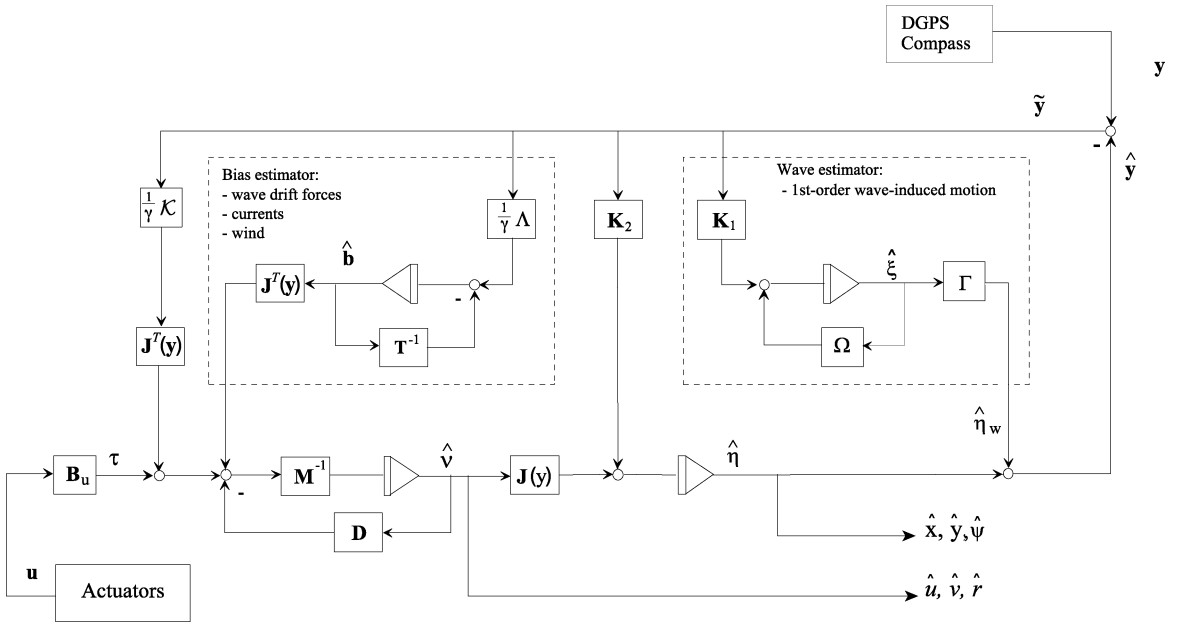

Fig. 3. Block diagram showing the nonlinear observer.

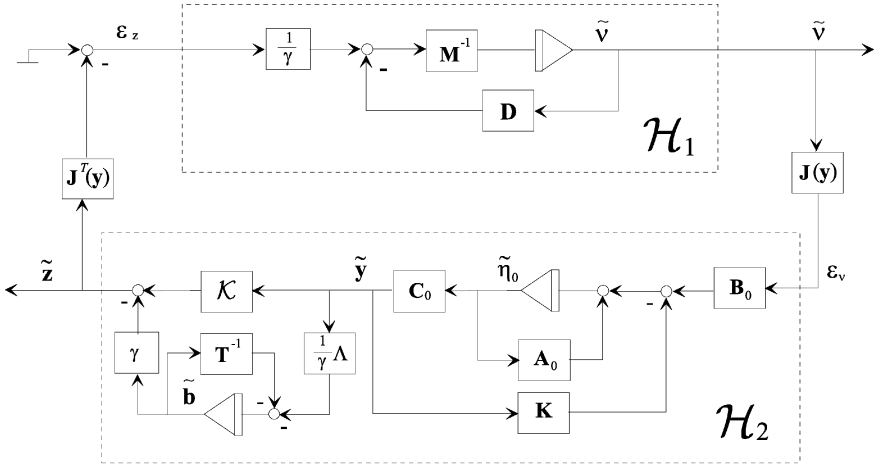

Fig. 4. Block diagram showing the dynamics of the position/bias and velocity estimation errors.

By defining

$$\tilde{\boldsymbol{x}} \triangleq \begin{bmatrix} \tilde{\boldsymbol{\eta}}_0 \\ \tilde{\boldsymbol{b}} \end{bmatrix}, \tag{34}$$

Eqs. (30), (31) and (34) can be written in compact form as

$$\dot{\tilde{\boldsymbol{x}}} = \boldsymbol{A}\tilde{x} + \boldsymbol{B}\boldsymbol{J}(\boldsymbol{y})\tilde{\boldsymbol{v}}, \tag{35}$$

$$\tilde{\boldsymbol{z}} = \boldsymbol{C}\tilde{\boldsymbol{x}}, \tag{36}$$

where

$$\boldsymbol{A} = \begin{bmatrix} \boldsymbol{A}_0 - \boldsymbol{K}\boldsymbol{C}_0 & \boldsymbol{0} \\ -\frac{1}{\gamma}\boldsymbol{\Lambda}\boldsymbol{C}_0 & -\boldsymbol{T}^{-1} \end{bmatrix}, \qquad \boldsymbol{B} = \begin{bmatrix} \boldsymbol{B}_0 \\ \boldsymbol{0} \end{bmatrix},$$

$$\boldsymbol{C} = [\mathscr{K}\boldsymbol{C}_0 \quad -\gamma\boldsymbol{I}]. \tag{37}$$

The error dynamics is shown in Fig. 4 where two new error terms $\boldsymbol{\varepsilon}_z = -\boldsymbol{J}^{\mathrm{T}}(\boldsymbol{y})\tilde{\boldsymbol{z}}$ and $\boldsymbol{\varepsilon}_v = \boldsymbol{J}(\boldsymbol{y})\tilde{\boldsymbol{v}}$ are defined.

5. Stability analysis

In this section both GES (Section 5.1) and passivity (Section 5.2) of the observer are proven.

5.1. SPR-Lyapunov function analysis

Lemma 1 (Kalman–Yakubovich–Popov (KYP) lemma). *Let* $Z(s) = \mathscr{C}(sI - \mathscr{A})^{-1}\mathscr{B}$ *be a* $n \times n$ *transfer function matrix, where* $\mathscr{A}$ *is Hurwitz,* $(\mathscr{A}, \mathscr{B})$ *is controllable, and*

$(\mathscr{A}, \mathscr{C})$ *is observable. Then,* $Z(s)$ *is strictly positive real (SPR) if and only if there exist positive-definite matrices* $\mathscr{P} = \mathscr{P}^{\mathrm{T}}$ *and* $\mathscr{Q} = \mathscr{Q}^{\mathrm{T}}$ *such that (Khalil, 1996)*

$$\mathscr{P}\mathscr{A} + \mathscr{A}^{\mathrm{T}}\mathscr{P} = -\mathscr{Q}, \tag{38}$$

$$\mathscr{B}^{\mathrm{T}}\mathscr{P} = \mathscr{C}. \tag{39}$$

Proposition 1 (SPR velocity estimation error). *If* $\gamma > 0$ *and the observer gain matrices are given the following structure*:

$$\boldsymbol{K}_1 = \begin{bmatrix} k_{11} & 0 & 0 \\ 0 & k_{12} & 0 \\ 0 & 0 & k_{13} \\ k_{21} & 0 & 0 \\ 0 & k_{22} & 0 \\ 0 & 0 & k_{23} \end{bmatrix}, \qquad \mathscr{K} = \begin{bmatrix} \kappa_1 & 0 & 0 \\ 0 & \kappa_2 & 0 \\ 0 & 0 & \kappa_3 \end{bmatrix}, \tag{40}$$

$$\boldsymbol{K}_2 = \begin{bmatrix} k_{31} & 0 & 0 \\ 0 & k_{32} & 0 \\ 0 & 0 & k_{33} \end{bmatrix}, \qquad \boldsymbol{\Lambda} = \begin{bmatrix} \lambda_1 & 0 & 0 \\ 0 & \lambda_2 & 0 \\ 0 & 0 & \lambda_3 \end{bmatrix}, \tag{41}$$

then the elements $k_{ij} > 0$, $\kappa_i > 0$ *and* $\lambda_i > 0$ *can be chosen such that the triple* $(\boldsymbol{A}, \boldsymbol{B}, \boldsymbol{C})$ *given by Eq.* (37), *that is the mapping* $\boldsymbol{\varepsilon}_v \mapsto \tilde{\boldsymbol{z}}$ *satisfies the KYP lemma.*

Proof. Since $\mathscr{K}$ and $\boldsymbol{\Lambda}$ are chosen to be diagonal, the mapping $\boldsymbol{\varepsilon}_v \mapsto \tilde{\boldsymbol{z}}$ (see the lower block in Fig. 4) can be described by three decoupled transfer functions

$$\tilde{\boldsymbol{z}}(s) = \boldsymbol{H}(s)\varepsilon_v(s) \quad \text{where } \boldsymbol{H}(s) = \boldsymbol{H}_0(s)\boldsymbol{H}_B(s)$$

and

$$\boldsymbol{H}_0(s) = \boldsymbol{C}_0(s\boldsymbol{I} + \boldsymbol{A}_0 - \boldsymbol{K}\boldsymbol{C}_0)^{-1}\boldsymbol{B}_0,$$

$$\boldsymbol{H}_B(s) = \mathscr{K} + (s\boldsymbol{I} + \boldsymbol{T}^{-1})^{-1}\boldsymbol{\Lambda}.$$

The diagonal structure of $\boldsymbol{H}(s)$ is shown in Fig. 5. The transfer functions $h_0^i(s)$ $(i = 1\text{–}3)$ of $\boldsymbol{H}_0(s)$ and $h_B^i(s)$ $(i = 1\text{–}3)$ of $\boldsymbol{H}_B(s)$ becomes

$$h_0^i(s) = \frac{s^2 + 2\zeta_i\omega_{oi}s + \omega_{oi}^2}{s^3 + (k_{2i} + k_{3i} + 2\zeta_i\omega_{oi})s^2 + (\omega_{oi}^2 + 2\zeta_i\omega_{oi}k_{3i} - k_{1i}\omega_{oi}^2)s + \omega_{oi}^2 k_{3i}}, \tag{42}$$

$$h_B^i(s) = \kappa_i \frac{s + (1/T_i + (\lambda_i/\kappa_i))}{s + 1/T_i} \overset{T_i \gg 1}{\approx} \kappa_i \frac{s + \lambda_i/\kappa_i}{s + 1/T_i}. \tag{43}$$

In order to obtain the desired notch effect (wave filtering) of the observer, see Definition 1, the desired shape of $h_0^i(s)$ is specified as

$$h_{0d}^i(s) = \frac{s^2 + 2\zeta_i\omega_{oi}s + \omega_{oi}^2}{(s^2 + 2\zeta_{\mathrm{n}i}\omega_{oi}s + \omega_{oi}^2)(s + \omega_{\mathrm{c}i})} \tag{44}$$

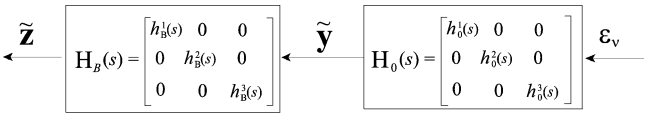

Fig. 5. The decoupled transfer function structure of the position error dynamics.

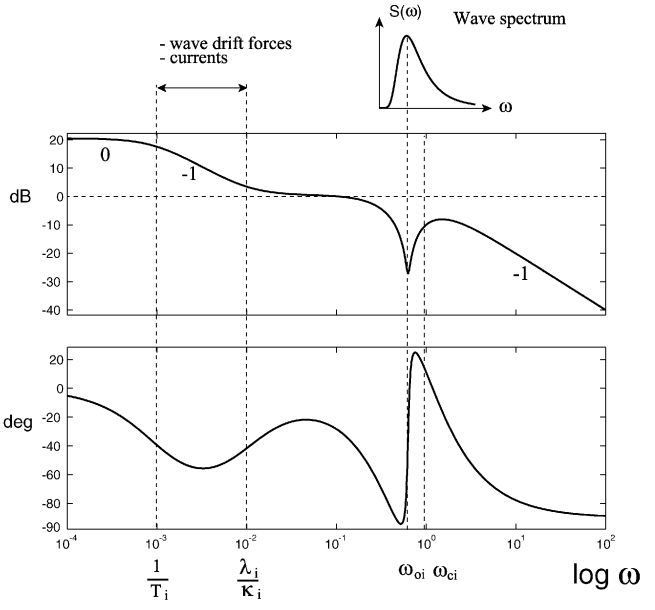

Fig. 6. Bode plot showing the transfer functions $h^i(s)$ when $1/T_i \ll \lambda_i/\kappa_i < \omega_{oi}\omega_{ci}$ $(i = 1\text{–}3)$.

where $\zeta_{\mathrm{n}i} > \zeta_i$ determines the notch and $\omega_{\mathrm{c}i} > \omega_{oi}$ is the filter cut-off frequency. Equating Eqs. (42) and (44) yields the following formulas for the filter gains in $\boldsymbol{K}_1$ and $\boldsymbol{K}_2$:

$$k_{1i} = -2\omega_{\mathrm{c}i}(\zeta_{\mathrm{n}i} - \zeta_i)\frac{1}{\omega_{oi}}, \tag{45}$$

$$k_{2i} = 2\omega_{oi}(\zeta_{\mathrm{n}i} - \zeta_i), \tag{46}$$

$$k_{3i} = \omega_{\mathrm{c}i}. \tag{47}$$

Notice that the filter gains can be gain-scheduled with respect to the dominating wave frequencies ω_{oi} if desired. In Fig. 6 the total transfer function $h^i(s) = h_B^i(s) \cdot h_0^i(s)$ is illustrated when all filter gains are properly selected. It is important that the three decoupled transfer functions $h^i(s)$ all have phase greater than -90° in order to meet the SPR requirement. It turns out that the KYP lemma and therefore the SPR requirement can easily be satisfied if the following tuning rules for T_i, λ_i and κ_i are applied:

$$1/T_i \ll \lambda_i/\kappa_i < \omega_{oi} < \omega_{\mathrm{c}i} \quad (i = 1\text{–}3). \tag{48}$$

Here ω_{oi} $(i = 1\text{–}3)$ are the dominating wave frequencies and $T_i \gg 1$ $(i = 1\text{–}3)$ are the bias time constants used to specify the limited integral effect in the bias estimator. □

Remark 2. The observer can be gain-scheduled with respect to the dominating wave frequency vector $\boldsymbol{\omega}_o = [\omega_{o1}, \omega_{o2}, \omega_{o3}]^{\mathrm{T}}$ by noticing that $\boldsymbol{K}_1 = \boldsymbol{K}_1(\boldsymbol{\omega}_o)$, see Eqs. (45) and (46). The gain matrices $\boldsymbol{K}_2$, $\boldsymbol{\Lambda}$ and $\mathscr{K}$ are independent of $\boldsymbol{\omega}_o$. An estimate of $\boldsymbol{\omega}_o$ can be found by using an on-line frequency tracker (Fossen, 1994).

Theorem 1 (Main result: globally exponentially stable nonlinear observer). *Under Assumptions A1–A4 the nonlinear observer given by* (22)–(26) *is globally exponentially stable.*

Proof. Consider the following Lyapunov function candidate:

$$V = \gamma \tilde{\boldsymbol{v}}^{\mathrm{T}} \boldsymbol{M} \tilde{\boldsymbol{v}} + \tilde{\boldsymbol{x}}^{\mathrm{T}} \boldsymbol{P} \tilde{\boldsymbol{x}}. \tag{49}$$

Differentiation of V along the trajectories of $\tilde{\boldsymbol{v}}$ and $\tilde{\boldsymbol{x}}$ and application of Assumptions A1–A4, yields

$$\dot{V} = -\gamma \tilde{\boldsymbol{v}}^{\mathrm{T}} (\boldsymbol{D} + \boldsymbol{D}^{\mathrm{T}}) \tilde{\boldsymbol{v}} + \tilde{\boldsymbol{x}}^{\mathrm{T}} (\boldsymbol{P}\boldsymbol{A} + \boldsymbol{A}^{\mathrm{T}}\boldsymbol{P}) \tilde{\boldsymbol{x}} + 2\tilde{\boldsymbol{v}}^{\mathrm{T}} \boldsymbol{J}^{\mathrm{T}}(\boldsymbol{y}) \boldsymbol{B}^{\mathrm{T}} \boldsymbol{P} \tilde{\boldsymbol{x}} - 2\tilde{\boldsymbol{v}}^{\mathrm{T}} \boldsymbol{J}^{\mathrm{T}}(\boldsymbol{y}) \tilde{\boldsymbol{z}}. \tag{50}$$

Application of Proposition 1 to Eq. (50), yields

$$\dot{V} = -\gamma \tilde{\boldsymbol{v}}^{\mathrm{T}} (\boldsymbol{D} + \boldsymbol{D}^{\mathrm{T}}) \tilde{\boldsymbol{v}} - \tilde{\boldsymbol{x}}^{\mathrm{T}} \boldsymbol{Q} \tilde{\boldsymbol{x}}. \tag{51}$$

Hence, $\tilde{\boldsymbol{v}}$ and $\tilde{\boldsymbol{x}} = [\tilde{\boldsymbol{\xi}}^{\mathrm{T}}, \tilde{\boldsymbol{\eta}}^{\mathrm{T}}, \boldsymbol{b}^{\mathrm{T}}]^{\mathrm{T}}$ converge exponentially to zero. □

5.2. Passivity interpretation of the nonlinear observer

The error dynamics in Fig. 4 can be described as illustrated in Fig. 7 by letting $\mathscr{H}_1$ denote the mapping $\boldsymbol{\varepsilon}_z \mapsto \tilde{\boldsymbol{v}}$ and $\mathscr{H}_2$ denote the mapping $\boldsymbol{\varepsilon}_v \mapsto \tilde{\boldsymbol{z}}$. Notice that the coordinate transformation is performed through a nonsingular and bounded matrix $\boldsymbol{J}(\boldsymbol{y})$.

Proposition 2 (Strictly passive velocity error dynamics). *The mapping $\mathscr{H}_1$ is state strictly passive.*

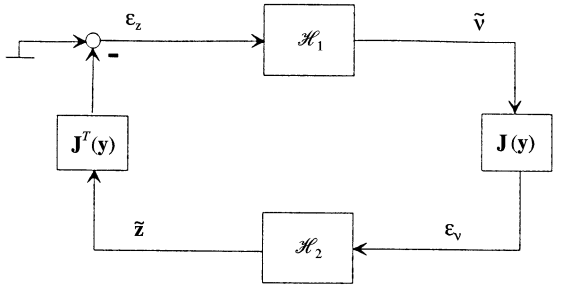

Fig. 7. The observer error dynamics in terms of two interconnected feedback error systems $\mathscr{H}_1$ (velocity) and $\mathscr{H}_2$ (position and bias).

Proof. Let

$$U = \tfrac{1}{2} \gamma \tilde{\boldsymbol{v}}^{\mathrm{T}} \boldsymbol{M} \tilde{\boldsymbol{v}} \tag{52}$$

be a positive-definite storage function. Time differentiation of U along the trajectories of $\tilde{\boldsymbol{v}}$ yields

$$\dot{U} = -\tfrac{1}{2} \gamma \tilde{\boldsymbol{v}}^{\mathrm{T}} (\boldsymbol{D} + \boldsymbol{D}^{\mathrm{T}}) \tilde{\boldsymbol{v}} - \tilde{\boldsymbol{z}}^{\mathrm{T}} \boldsymbol{J}(\boldsymbol{y}) \tilde{\boldsymbol{v}}. \tag{53}$$

Using the fact that $\boldsymbol{\varepsilon}_z = -\boldsymbol{J}^{\mathrm{T}}(\boldsymbol{y}) \tilde{\boldsymbol{z}}$, yields

$$\boldsymbol{\varepsilon}_z^{\mathrm{T}} \tilde{\boldsymbol{v}} = \dot{U} + \tfrac{1}{2} \gamma \tilde{\boldsymbol{v}}^{\mathrm{T}} (\boldsymbol{D} + \boldsymbol{D}^{\mathrm{T}}) \tilde{\boldsymbol{v}}. \tag{54}$$

Hence,

$$\int_{t_0}^{t} \boldsymbol{\varepsilon}_z^{\mathrm{T}}(\tau) \tilde{\boldsymbol{v}}(\tau)\, \mathrm{d}\tau \geq \alpha \tilde{\boldsymbol{v}}^{\mathrm{T}} \tilde{\boldsymbol{v}} + \beta, \tag{55}$$

where $\alpha = \frac{1}{2} \gamma \lambda_{\min}(\boldsymbol{M})$ is a positive constant and $\beta = \frac{1}{2}\gamma \int_{t_0}^{t} \tilde{\boldsymbol{v}}^{\mathrm{T}} (\boldsymbol{D} + \boldsymbol{D}^{\mathrm{T}}) \tilde{\boldsymbol{v}} \mathrm{d}\tau \geq 0$ is the dissipated energy due to hydrodynamic damping. □

Theorem 2 (Passive observer). *The nonlinear observer* (22)–(26) *is passive.*

Proof. Since it is established that $\mathscr{H}_1$ is state strictly passive and $\mathscr{H}_2$ is SPR (Propositions 1 and 2), the nonlinear observer (22)–(26) must be passive. In addition to this, GES has been shown (Theorem 1). □

6. Case study

Both computer simulations and full-scale experiments have been used to evaluate the performance and robustness of the nonlinear passive observer. The case studies are based on the following models of the ship–bias–wave system:

$$\boldsymbol{M} = \begin{bmatrix} 5.3122 \times 10^6 & 0 & 0 \\ 0 & 8.2831 \times 10^6 & 0 \\ 0 & 0 & 3.7454 \times 10^9 \end{bmatrix}, \tag{56}$$

$$\boldsymbol{D} = \begin{bmatrix} 5.0242 \times 10^4 & 0 & 0 \\ 0 & 2.7229 \times 10^5 & -4.3933 \times 10^6 \\ 0 & -4.3933 \times 10^6 & 4.1894 \times 10^8 \end{bmatrix}. \tag{57}$$

A picture of the actual ship is shown in Fig. 8.

The length of *Northern Clipper* is $L = 76.2$ m and the mass is $m = 4.591 \times 10^6$ kg. The coordinate system is located in the center of gravity. The bias time constants were chosen as

$$\boldsymbol{T} = \begin{bmatrix} 1000 & 0 & 0 \\ 0 & 1000 & 0 \\ 0 & 0 & 1000 \end{bmatrix}. \tag{58}$$

Fig. 8. Northern Clipper. A multipurpose supply vessel owned by Sævik Supply Management, Norway.

The wave model parameters were chosen as $\zeta_i = 0.1$ and $\omega_{oi} = 0.8976$ rad/s corresponding to a wave period of 7.0 s in surge, sway and yaw. The notch filter parameters were chosen as $\zeta_{ni} = 1.0$ and $\omega_{ci} = 1.1$. From Eqs. (45)–(47) we get

$$\boldsymbol{K}_1 = \begin{bmatrix} -2.2059 & 0 & 0 \\ 0 & -2.2059 & 0 \\ 0 & 0 & -2.2059 \\ 1.6157 & 0 & 0 \\ 0 & 1.6157 & 0 \\ 0 & 0 & 1.6157 \end{bmatrix},$$

$$\boldsymbol{K}_2 = \begin{bmatrix} 1.1 & 0 & 0 \\ 0 & 1.1 & 0 \\ 0 & 0 & 1.1 \end{bmatrix}. \tag{59}$$

The last two gain matrices and γ were chosen as

$$\boldsymbol{\mathcal{K}} = \begin{bmatrix} 0.1 & 0 & 0 \\ 0 & 0.1 & 0 \\ 0 & 0 & 0.01 \end{bmatrix}, \qquad \boldsymbol{\Lambda} = 0.1\boldsymbol{\mathcal{K}}, \qquad \gamma = 1. \tag{60}$$

Both the simulation study and the full-scale experiment were performed with a measurement frequency of 1 Hz. The simulation study was performed with nonzero noise terms $\boldsymbol{n}$, $\boldsymbol{d}$ and $\boldsymbol{w}$ even though these terms were assumed to be zero in the Lyapunov analysis. This was done to demonstrate the excellent performance of the observer in the presence of stochastic noise.

6.1. Simulation study

In the simulation study the control inputs were chosen as

$$\boldsymbol{\tau} = \begin{bmatrix} 1000\sin(0.05t) \\ 1000\sin(0.1t) \\ 1000\sin(0.07t) \end{bmatrix}, \tag{61}$$

The amplitudes of the first-order wave-induced motion in surge, sway and yaw were limited to 1.0 m, 1.0 m and 1.0°, respectively. These disturbances were added to the positions and heading measurements in the simulator.

The simulation results are shown in Figs. 9–11. The first-order wave-induced motion in surge, sway and yaw

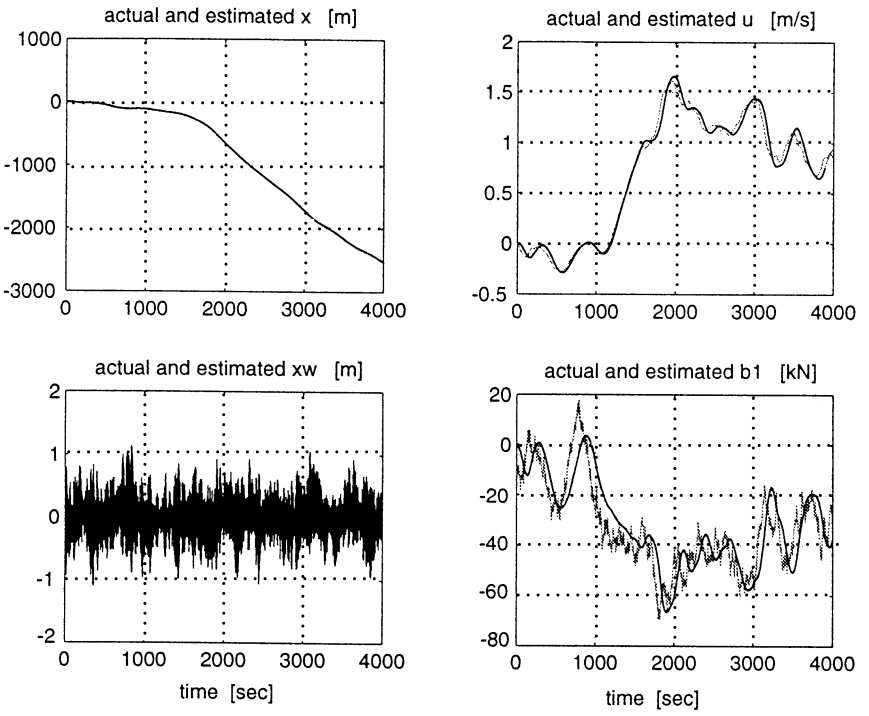

Fig. 9. Simulation study: position, velocity, wave disturbance and bias (grey), and their estimates (black) in surge.

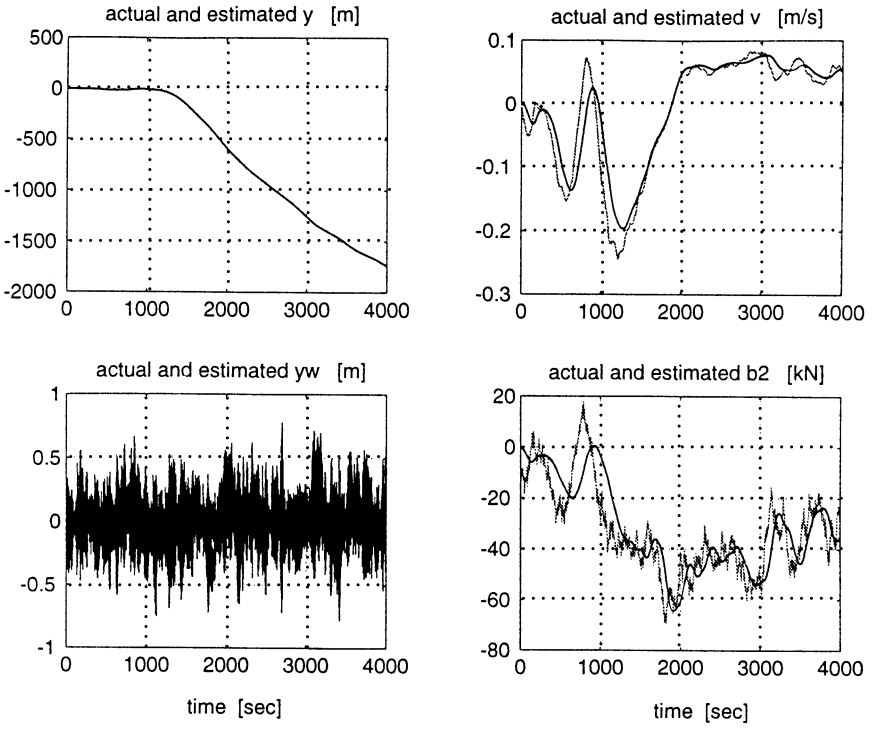

Fig. 10. Simulation study: position, velocity, wave disturbance and bias (grey), and their estimates (black) in sway.

and their estimates are shown in the lower left plots. It is seen that excellent tracking of the position, velocity and bias is obtained even though the measurements are highly noise-corrupted. In particular, it is impressing that the stochastic behavior of the bias is estimated as well. This means that the zero white noise assumption in the proof can be relaxed when implementing the observer.

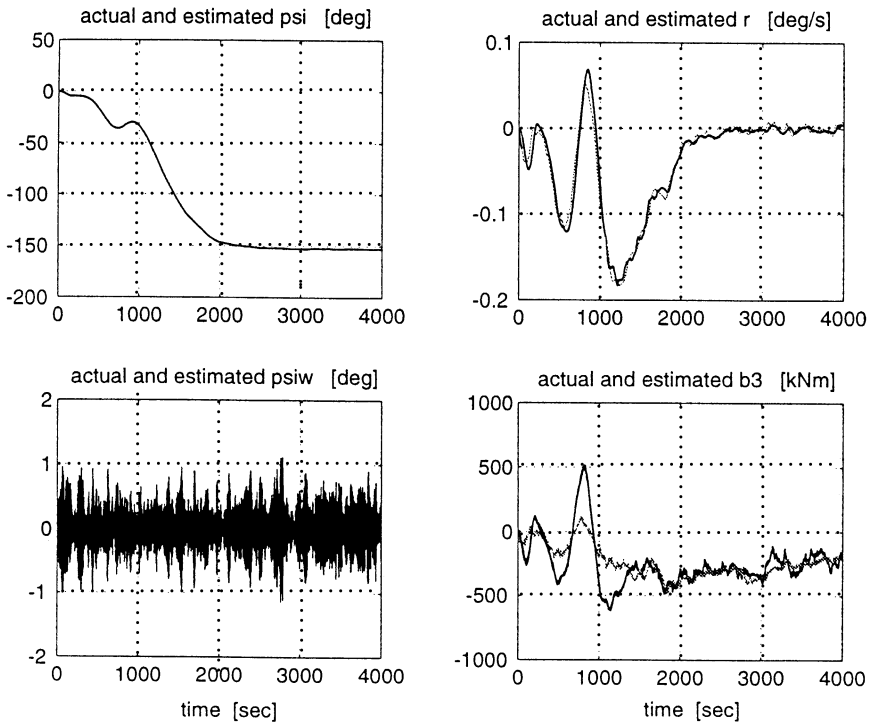

Fig. 11. Simulation study: heading angle, angular rate, wave disturbance and bias (grey), and their estimates (black) in sway.

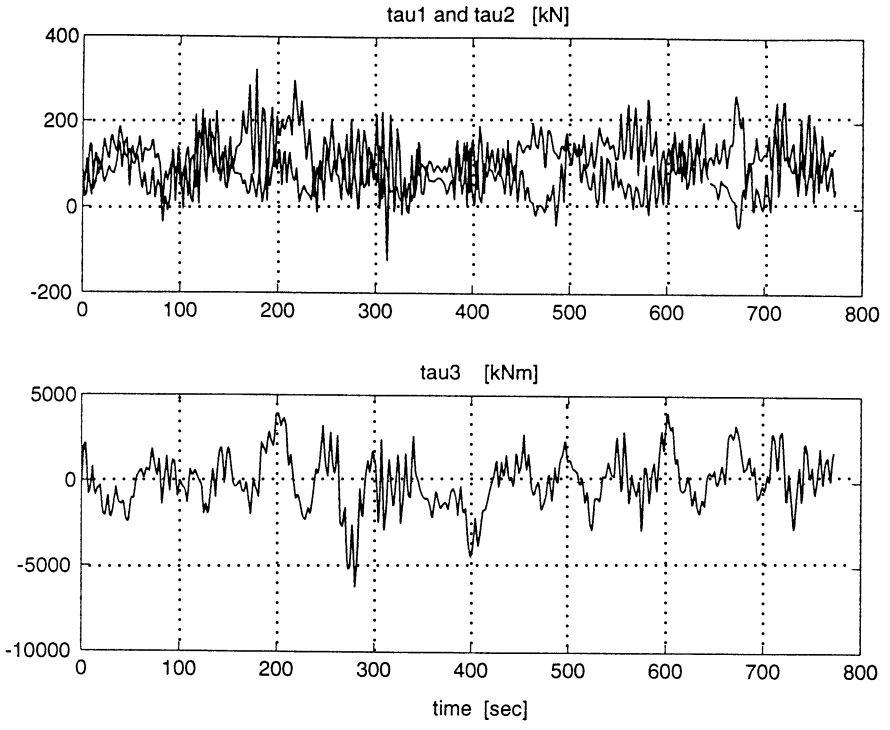

Fig. 12. Experimental data: control inputs in surge, sway and yaw.

6.2. Experimental results

The simulated observer was implemented on Northern Clipper (Fig. 8) to investigate the performance and robustness on "real" data. The time series from the full-scale experiments are shown in Figs. 12–14. The experiments were performed in an extreme weather situation to demonstrate the filtering properties. The

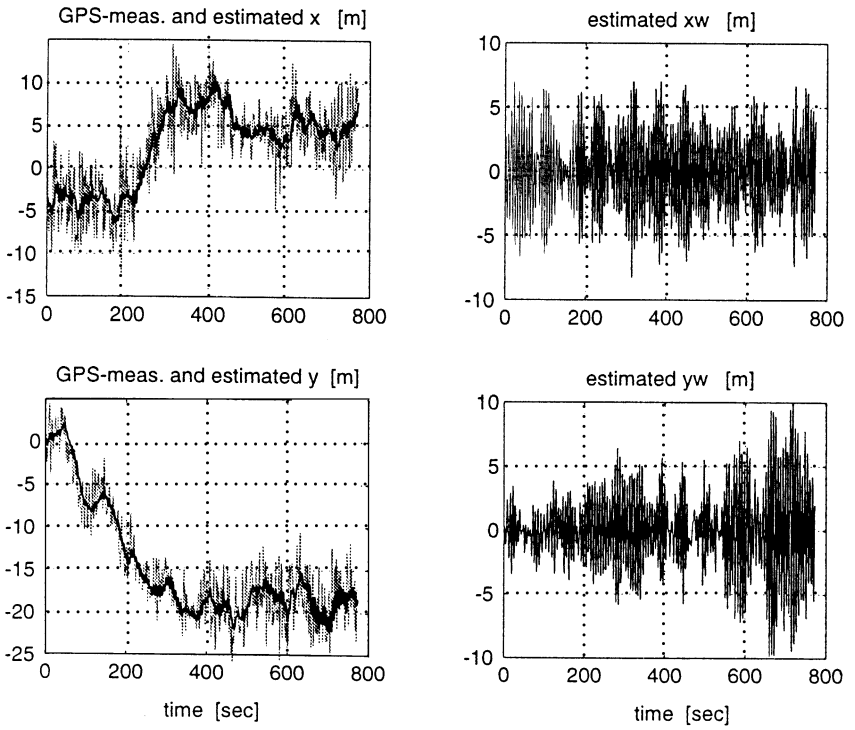

Fig. 13. Experimental data: actual LF + WF position (grey) with estimates (black) of the LF- and WF-position components in surge and sway.

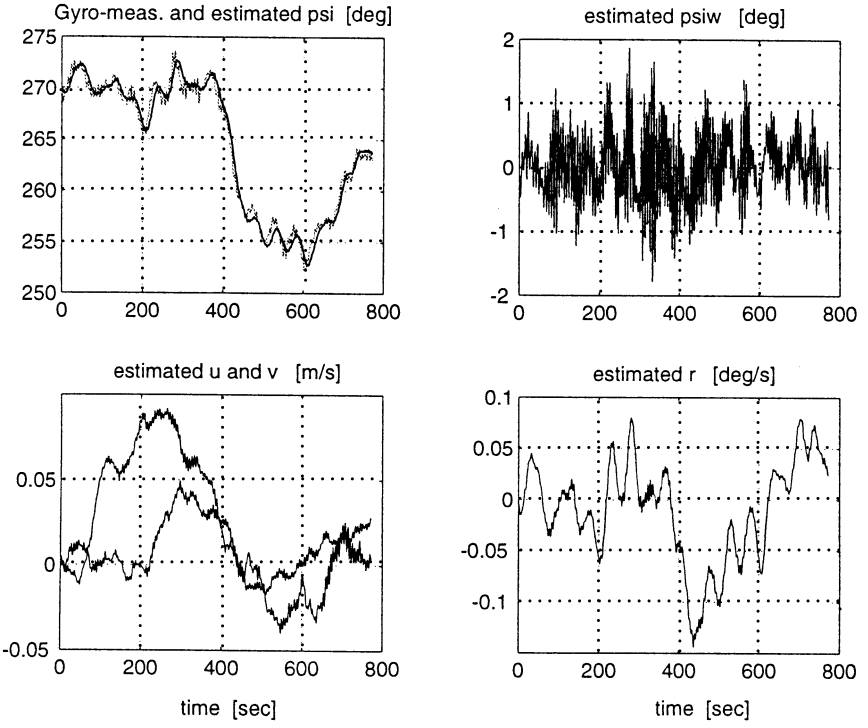

Fig. 14. Experimental data: upper plots — actual LF + WF heading angle (grey) with estimates (black) of the LF- and WF-heading angles. Lower plots — estimates of the LF velocities in surge, sway and yaw.

amplitudes of the first-order wave-induced motion in surge, sway and yaw were as large as 8.0 m, 10.0 m and 2.0°, respectively. This corresponds to sea state codes 8 and 9 (very high or phenomenal seas). Again, excellent results were obtained. It is seen from the plots that most of the first-order wave disturbances are filtered out resulting in smooth estimates of the positions, heading and velocities. Hence, the feedback controller

should not be to much affected by the rough weather condition.

7. Conclusions

In this paper a nonlinear passive observer for ships in surge, sway and yaw has been derived. The observer is proven to be global exponential stable and passive. The number of tuning parameters has been reduced to a minimum by using passivity theory. It has been shown that both the low-frequency position and velocity of the ship together with accurate bias state estimates (environmental disturbances) can be computed from noisy position measurements. In addition, filtering of first-order wave-induced disturbances has been done.

The nonlinear passive observer has been simulated on a computer model of a supply vessel and implemented on a full-scale supply vessel (Northern Clipper) with excellent results. The simulation results showed that all estimation errors including the bias estimation errors converged exponentially to zero. Experimental results from sea trials performed in the North Sea have also been reported.

The main advantage of the nonlinear design to a linear design is that the kinematic equations of motion do not have to be linearized about a set of predefined constant yaw angles, typically 36 operating points in steps of 10°, to cover the whole heading envelope of the ship. This is, however, common when using linear Kalman filters and gain scheduling techniques. In addition, it is shown that the tuning procedure is relatively simple to perform due to the passive structure of the observer. On the contrary, it is quite time consuming to tune the Kalman filter since the weighting matrices will be of dimension 15×15 and 3×3 corresponding to the estimation error and control input vectors, respectively.

The results of the paper have applicability to dynamic positioning (DP), tracking control and berthing of ships as well as other marine craft. Future work will look into the design of a nonlinear control law utilizing the passive structure of the observer.

Acknowledgements

The authors are grateful to Dr. Asgeir J. Sørensen and co-workers at ABB Industri AS in Oslo for valuable comments, discussion and help with the sea trials.

References

Aarset, M. F., Strand, J. P., & Fossen, T. I. (1998). Nonlinear vectorial observer backstepping with integral action and wave filtering for ships. *Proc. the IFAC Conf. on Control Applications in Marine System (CAMS'98)*, Fukuoka, Japan, 27–20 October.

Balchen, J. G., Jenssen, N. A., & Sælid, S. (1976). Dynamic positioning using Kalman filtering and optimal control theory. *Proc. IFAC/IFIP Symp. on Automation in Offshore Oil Field Operation*, Holland, Amsterdam, pp. 183–186.

Balchen, J. G., Jenssen, N. A., & Sælid, S. (1980a). Dynamic positioning of floating vessels based on Kalman filtering and optimal control. *Proc. 19th IEEE Conf. on Decision and Control*, New York, NY, pp. 852–864.

Balchen, J. G., Jenssen, N. A., & Sælid, S. (1980b). A dynamic postioning system based on Kalman filtering and optimal control. *Modeling, Identification Control*, *MIC-1*(3), 135–163.

Fossen, T. I. (1994). *Guidance and control of ocean vehicles*. New York: Wiley.

Fossen, T. I., & Grøvlen, Å. (1998). Nonlinear output feedback control of dynamically positioned ships using vectorial observer backstepping. *IEEE Trans. Control Systems Technology*, *TCST-6*(1), 121–128.

Fossen, T. I., Sagatun, S. I., & Sørensen, A. J. (1996). Identification of dynamically positioned ships. *J. Control Engng Practice*, *JCEP-4*(3), 369–376.

Fung, P. T.-K., & Grimble, M. (1983). Dynamicship positioning using self-tuning Kalman filter. *IEEE Trans. Automat. Control*, *TAC-28*(3), 339–349.

Grimble, M. J., Patton, R. J., & Wise, D. A. (1980a). The design of dynamic ship positioning control systems using stochastic optimal control theory. *Opt. Control Appl. Methods*, *OCAM-1*, 167–202.

Grimble, M. J., Patton, R. J., & Wise, D. A. (1980b). Use of Kalman filtering techniques in dynamic ship positioning systems. *IEE Proc., Pt.D*, *127*(3) 93–102.

Hoffman-Wellenhof, B., Lichtenegger, H., & Collins, J. (1994). *GPS theory and practice*. New York: Springer.

Khalil, H. K. (1996). *Nonlinear systems*. Englewood Cliffs. NJ: Prentice-Hall.

Loria, A., Fossen, T. I., & Panteley, E. (1998). Nonlinear global output feedback control of ships using the separation principle. *IEEE Trans. Control Systems Technology* (submitted).

Parkinson, B. (ed.) (1996). *Global positioning system: Theory and applications*. Washington: American Institute of Aeronautics and Astronautics, Inc.

The Society of Naval Architects and Marine Engineers — SNAME (1950). Nomenclature for treating the motion of a submerged body through a fluid. *Technical and Research Bulletin* No. 1–5.

Sælid, S., Jenssen, N. A., & Balchen, J. G. (1983). Design and analysis of a dynamic positioning system based on Kalman filtering and optimal control. *IEEE Trans. Automat. Control*, *TAC-28*(3), 331–339.

Sørensen, A. J., Sagatun, S. I., & Fossen, T. I. (1996). Design of a dynamic positioning system using model-based control. *J. Control Engng Practice*, *JCEP-4*(3), 359–368.

Triantafyllou, M. S., Bodson, M., & Athans, M. (1983). Real time estimation of ship motions using Kalman filtering techniques. *IEEE J. Oceanic Engng*, *JOE-8*(1), 3–14.

Thor I. Fossen received the M.Sc. degree in Naval Architecture in 1987 from the Norwegian University of Science and Technology (NTNU), Trondheim and the Ph.D. degree in Engineering Cybernetics from NTNU in 1991. In the period 1989–1990 Fossen pursued postgraduate studies as a Fullbright scholar in flight control at the Department of Aeronautics and Astronautics, University of Washington, Seattle. In May 1993 Fossen was appointed as a professor in Guidance, Navigation and Control at the Department of Engineering Cybernetics at NTNU where he is teaching applied nonlinear and adaptive control.

Fossen is a Senior Scientific Advisor for ABB Industri, Marine Division in Oslo and he has participated in several industrial projects in the period 1993–1998. This includes dynamic positioning (DP) of free-floating and moored ships/platforms, nonlinear and passive state estimation, identification of ship dynamics, buoyancy control systems and navigation systems.

Fossen is the author of "Guidance and Control of Ocean Vehicles" (Wiley, 1994) and he is co-authoring "Underwater Robotic Vehicles: Design and Control" (TSI Press, 1995). He is the Vice Chairman of the IFAC Technical Committee on Marine System.

Jann Peter Strand was born in Norway in 1969. He received the M.Sc. degree in Electrical Engineering at the Norwegian University of Science and Technology (NTNU) in 1994. Since 1995 he has been studying towards a Ph.D. degree in Engineering Cybernetics at the Department of Engineering Cybernetics, NTNU.

After receiving his M.Sc. degree he held a control engineer position at ABB Industri ASA, Marine Division, working on development and implementation of ship positioning control systems. In 1997 he was a visiting scholar at the Center for Control Engineering and Computation at the University of California, Santa Barbara (UCSB). His research interests are nonlinear and adaptive control with application to dynamic positioning (DP) systems and thruster-assisted position mooring systems for ships.